Chemical Science

ROYAL SOCIETY OF CHEMISTRY

EDGE ARTICLE

View Article Online
View Journal | View Issue

Cite this: *Chem. Sci.*, 2025, **16**, 21583

All publication charges for this article have been paid for by the Royal Society of Chemistry

Received 25th September 2025
Accepted 9th October 2025

DOI: 10.1039/d5sc07444d

rsc.li/chemical-science

Excitation-dependent circularly polarized luminescence triggered by selective excitation of achiral dichroic dyes in cholesterol liquid crystals

Lulu Li,[a] Peiting Jiang,[a] Lei Chen,[a] Yang Li *[b] and Yixiang Cheng *[b]

Excitation-dependent (ExD) circularly polarized luminescence (CPL) holds great potential for applications in anti-counterfeiting and information encryption due to its low cost, ease of operation, and reversibility. In this study, we propose a strategy to obtain ExD CPL by selective excitation of dyes with distinct dichroism and excitation wavelengths in a chiral liquid crystal (CLC) host. *R*/*S*-CLC-PG doped with the green-emitting dye EG (negative dichroism, $S_F = -0.31$) and red-emitting PTZ (positive dichroism, $S_F = 0.15$) can emit green CPL (−0.48/0.37 at 530 nm) at 365 nm excitation and inverted red CPL (0.53/−0.53 at 620 nm) at 420 nm excitation. In addition, *R*/*S*-CLC-PR doped with PTZ and red-emitting dye ER (negative dichroism, $S_F = -0.30$) can emit red CPL (−0.16/0.13 at 620 nm) at 365 nm excitation and inverted red CPL (0.52/−0.55 at 620 nm) at 420 nm excitation. This work presents a versatile platform for developing ExD CPL materials with potential applications in anti-counterfeiting devices.

Introduction

Counterfeit products have emerged as a serious menace that exerts detrimental impacts on multiple crucial aspects, including the global economy, national security, and human health.[1–3] Over the past few decades, in order to combat the rampant problem of counterfeiting, a vast number of anti-counterfeiting technologies have been painstakingly developed.[4–7] Circularly polarized luminescence (CPL) has emerged as an area with high potential within the anti-counterfeiting field, particularly in the domain of information security.[8–12] CPL-based anti-counterfeiting techniques take advantage of the unique optical properties of materials to encode and decode information in a manner that is extremely difficult for counterfeiters to mimic. The distinctive polarization characteristics of CPL can be utilized to generate secure markings or labels, which can be precisely detected and verified by means of specialized optical devices.[13–15]

The excitation-dependent (ExD) CPL material is a type of CPL material whose CPL signal can respond to the excitation wavelength.[16–19] This responsiveness imparts an additional level of complexity and security to the anti-counterfeiting process, enabling a dynamic and multi-level authentication mechanism.[20–23] When such materials are integrated into anti-counterfeiting systems, it becomes even more arduous for counterfeiters to replicate or circumvent the authentication process. In 2022, Liu's group reported an ExD-CPL material based on helical nanostructures derived from chiral tartaric acylhydrazone derivatives.[24] Notably, the emission wavelength could not only be tuned by the excitation wavelength, but the handedness of the CPL could also be modulated in either an inverted or ON/OFF manner. More recently, they further developed an ExD circularly polarized phosphorescence (CPP) material within a supramolecular gel system.[25] In 2024, Ding *et al.* reported ExD-CPL from chiral emissive metal–organic frameworks doped with ExD dyes, enabling effective chirality transfer.[26] However, there are still two problems that need to be overcome in the ExD CPL area: firstly, it is essential to enhance the g_{lum} value. Secondly, a strategy should be developed to simultaneously achieve wavelength tunability and exert precise control over the CPL handedness for ExD-CPL materials.[27–29]

Using emissive cholesteric liquid crystals (CLCs) has been recognized as an effective approach for achieving high dissymmetry factor (g_{lum}) values through chiral supramolecular co-assembly.[30,31] This co-assembly typically forms an ordered, regular CLC texture, resulting in a pronounced CPL amplification effect in achiral dyes through intermolecular chirality transfer and induction mechanisms.[32–34] Inspired by common methods for achieving multicolor emission in organic light-emitting diodes-such as incorporating luminophores with different emission colors into a single polymer or constructing multiple emitting centers in a single-component molecular crystal to obtain multicolor emission at different excitation wavelengths,[35–38] we propose that ExD CPL can be achieved by incorporating multiple achiral emitting dyes into a CLC host. Moreover, by controlling the dichroism of achiral dyes, the

[a]School of Environmental and Chemical Engineering, Jiangsu University of Science and Technology, Changhui Street, Zhenjiang 212003, P. R. China. E-mail: lilulu0303@163.com

[b]School of Chemistry and Chemical Engineering, Nanjing University, Xianlin Avenue, Nanjing 210000, P. R. China. E-mail: yxcheng@nju.edu.cn

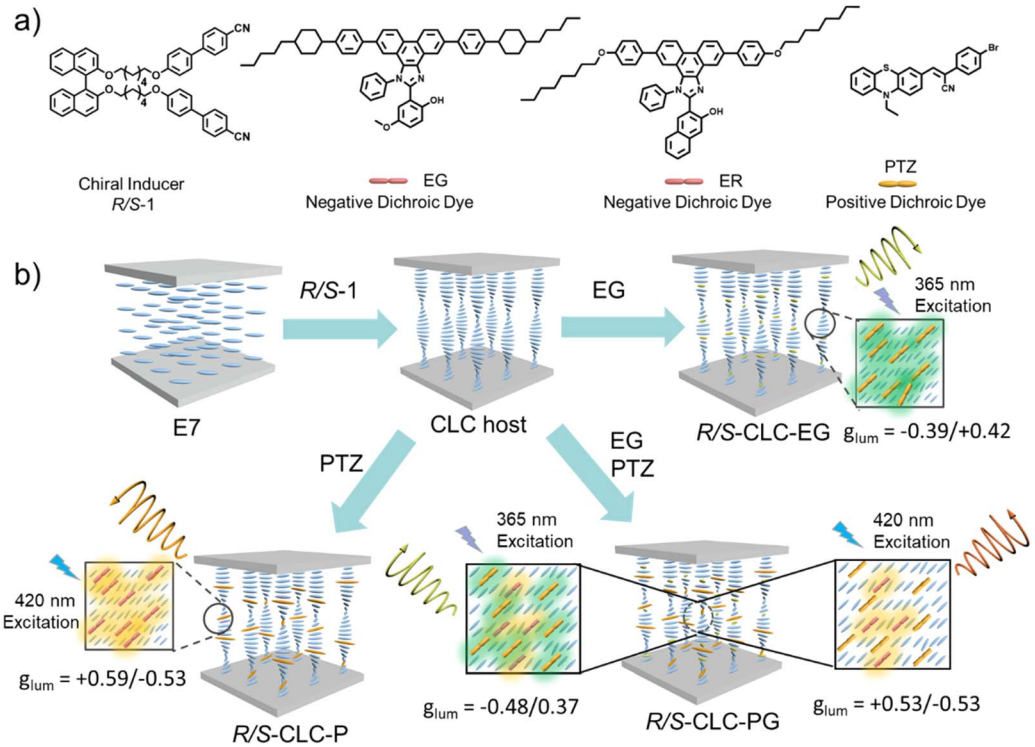

Scheme 1 (a) Molecular structures of chiral inducer *R*/*S*-1, positive dichroic dye PTZ and negative dichroic dyes EG and ER. (b) Schematic illustrations of the construction of an ExD CPL inversion system under 365 nm and 420 nm excitation.

handedness of CPL can be easily tuned in CLCs simultaneously due to the controllable TDM vector helix other than the CLC helix.[39,40]

To validate our hypothesis, we aim to prepare a multicomponent co-assembled CLC by doping multiple dyes (Scheme 1a) into a single CLC host. We first selected the excited-state intramolecular proton transfer (ESIPT) dyes EG ($S_F = -0.31$) and ER ($S_F = -0.30$) as examples of achiral negative dyes due to their unique emission process.[41,42] Due to the special proton transfer emission process, the negative dichroic dyes ER and EG can only be excited using UV light. In contrast, the positive dichroic dye PTZ ($S_F = 0.15$), a donor–acceptor dye with an intramolecular charge transfer (ICT) emission process, can be excited at both 365 nm and 420 nm, with emission occurring at 600 nm. By doping PTZ with ER in an appropriate ratio, the resulting *R*/*S*-CLC-PG can emit green CPL (−0.48/0.37 at 530 nm) at 365 nm excitation and inverted red CPL (0.53/−0.53 at 620 nm) at 420 nm excitation. Similarly, by doping PTZ with ER at an appropriate ratio, the resulting *R*/*S*-CLC-PR can emit red CPL (−0.16/0.13 at 620 nm) at 365 nm excitation and inverted red CPL (0.52/−0.55 at 620 nm) at 420 nm excitation. This strategy can be applied to construct ExD CPL that allows simultaneous control of the emission wavelength and CPL handedness by selecting excitation of dyes with a distinct excitation wavelength and dichroism. These dynamic CPL materials could be used for information encryption and anti-counterfeiting applications.

Results and discussion

The detailed synthesis procedures and characterization of EG, ER, and PTZ are provided in the SI. The photophysical properties of these compounds were studied in THF solutions at a concentration of 10^{-5} mol L^{-1} (Fig. 1 and S1). The excitation

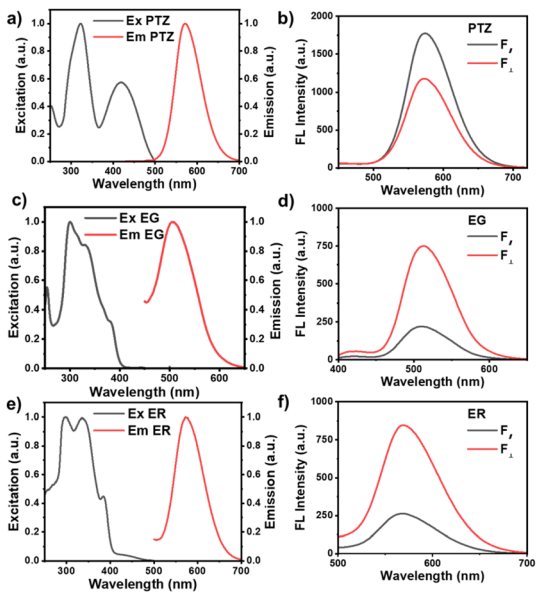

Fig. 1 Excitation and emission spectra of (a) PTZ, (c) EG and (e) ER. Polarized FL spectra of (b) PTZ, (d) EG and (f) ER.

spectrum of PTZ is shown in Fig. 1a, with an obvious excitation peak at 420 nm, which can be attributed to the ICT effect from phenothiazine to the *p*-bromophenylacetonitrile group.[43] The emission peak of PTZ is located at 575 nm. The ESIPT molecules EG and ER emit at 507 nm and 563 nm (very close to that of PTZ), respectively, in THF (Fig. 1c and e). In the ground state, these dyes exist in the enol form. Upon excitation, proton transfer occurs, producing the keto form in the excited state and resulting in a large apparent Stokes shift. Notably, the absorption spectra of these ESIPT derivatives are all confined to the UV region (Fig. S1), resulting in almost no spectral overlap between their absorption and emission bands.[44]

To verify the dichroism of the three dyes, quantified using the S_F value, the polarized fluorescence (FL) spectra of the achiral dyes were measured in a liquid crystal medium.[45] The emissive nematic liquid crystal (NLC) systems, NLC-PTZ, NLC-EG, and NLC-ER, were prepared by doping 1 wt% of PTZ, EG, and ER (Table S1), respectively, into the commercial NLC E7. After injecting the NLCs into aligned liquid crystal cells, the FL spectra parallel ($F_{\parallel}$) and perpendicular ($F_{\perp}$) to the molecular orientation were measured, as shown in Fig. 1. The stronger $F_{\parallel}$ emission intensity confirmed the positive dichroic nature of PTZ, with an S_F value of 0.15 (eqn (S1)).[46] The stronger $F_{\perp}$ emission intensity of EG and ER indicated their negative dichroic properties, with S_F values of −0.31 and −0.30, respectively. To further investigate the origin of the dichroic behavior of the achiral dyes, we performed density functional theory (DFT) calculations using the B3LYP/6-31G method with the Gaussian 09 program. The results, shown in Fig. S2, revealed that the TDM vectors for the ESIPT dyes EG and ER extend from the imidazole group to the carbonyl group. To enhance the negative dichroism of the ESIPT dyes, EG and ER were designed by attaching mesogenic units to the imidazoline ring in a direction perpendicular to the transition dipole moment (TDM) vector.[47]

The CLC can be prepared by incorporating the chiral inducer *R*/*S*-1 and achiral dyes into the commercially available NLC E7.[48] The doping concentrations of the chiral inducer and achiral dyes were optimized using PTZ and *R*-1 as examples, as shown in Fig. S3. *R*/*S*-CLC-P, *R*/*S*-CLC-EG, and *R*/*S*-CLC-ER were then prepared by doping 1 wt% of PTZ, 1 wt% of EG, and 1.0 wt% of ER into the E7 host with 1 wt% of *R*/*S*-1, respectively (Table S1). The chiroptical properties of these CLCs were measured by injecting them into 15 μm thick quartz cells, as illustrated in Fig. 2. The circular dichroism (CD) spectra revealed that CLCs-P exhibited a strong mirror-image effect and significant Cotton effects from 280 to 550 nm (Fig. 2a and S4). The band at 300 nm is attributed to the chiral co-assembly between the CLC host and PTZ,[49] while the strong absorption at 450 nm corresponds to the absorption of the PTZ dye itself. These pronounced CD signals are likely the result of efficient chiral transfer from the CLC host to the achiral dyes during the co-assembly process. Similarly, the CD signals of CLCs-EG and CLCs-ER (Fig. 2c and e) showed the same polarization as CLC-P in the 280 to 300 nm range, indicating that they share the same helical superstructure in the CLC host. However, for EG and ER, the CD signals from 370 to 400 nm exhibited opposite polarization, likely due

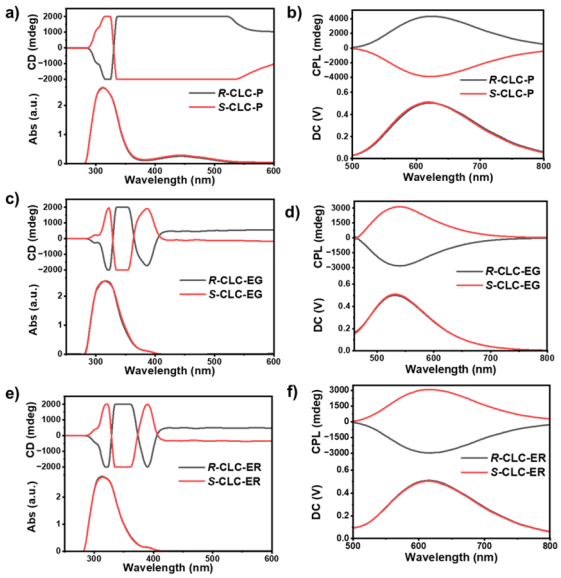

Fig. 2 CD and CPL spectra of (a and b) *R*/*S*-CLC-P, (c and d) *R*/*S*-CLC-EG and (e and f) *R*/*S*-CLC-ER.

to the negative dichroic nature of the ESIPT dyes (resulting in an inverted TDM helix).[50]

Next, the CPL spectra of the CLCs were measured. *R*/*S*-CLCs-P exhibited strong CPL signals with g_{lum} values of +0.59 and −0.53 at 620 nm, which corresponded well with the emission of PTZ (Fig. 1b). The red shift in the emission spectra is likely due to the polarity difference between the E7 host and THF.[51] *R*/*S*-CLCs-EG displayed strong CPL signals (g_{lum} = −0.39 and +0.42) at 530 nm (Fig. 2d and S5). Interestingly, CLCs-EG, with the same chiral inducer, showed opposite CPL polarizations. This behavior can be attributed to the different dichroic properties of the achiral dyes.[40] A similar trend was observed in the CPL spectra of CLCs-ER (g_{lum} = −0.41 and +0.43), with the CPL wavelength matching well with that of CLCs-P (Fig. 3f). The FL intensities of the CLCs exhibited clear differences under left- and right-handed circular polarization filters (L/R-CPFs), visible to the naked eye, confirming the large g_{lum} values of the CLCs (Fig. S6).[52]

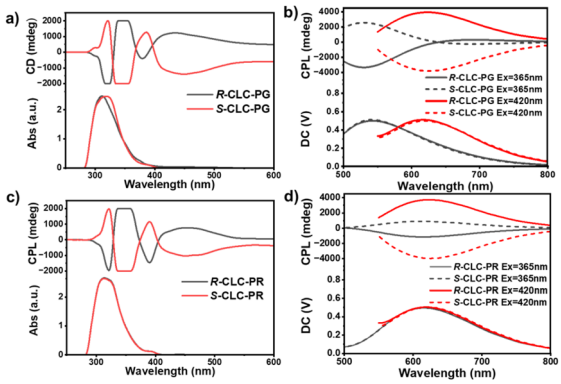

Fig. 3 CD and CPL spectra of (a and c) *R*/*S*-CLC-PG and (b and d) *R*/*S*-CLC-PR.

The POM images of the CLCs were examined to investigate their superstructure in detail. A characteristic fingerprint texture was observed in the CLCs (Fig. S7a–c), indicating the formation of a highly ordered helical superstructure through the co-assembly process.[53] The direction of the helix was confirmed by comparing the CLCs to natural CLCs, such as cholesteryl oleyl carbonate, which is known to exhibit a left-handed structure.[54,55] As shown in Fig. S7d–i, the schlieren texture observed at the contact zones of the *R*-CLCs and cholesteryl oleyl carbonate confirmed a right handed structure. Similarly, the *S*-CLCs exhibited a left-handed helix with a continuous pattern. These results demonstrate that the superstructure of the CLCs was not affected by the achiral dyes. The helical pitches were calculated to be 4.9, 5.3, 6.1, 4.7 and 4.9 μm, respectively, which are evidently larger than the range of the visible light region (Fig. S8). Based on these measurements, we can rule out the possibility that the effect of selective reflection plays a role in the CPL emission. This finding further confirmed that the CPL polarization of the CLCs could be controlled by the dichroism of the achiral dyes, despite the CLCs having the same helical structure.

Furthermore, achiral dyes PTZ, EG, and ER were co-doped into a single CLC to construct an ExD CPL material. The excitation and emission spectra of the individual CLCs are shown in Fig. S9. CLC-PTZ exhibited a clear excitation peak at 450 nm, consistent with its behavior in solution. In contrast, CLC-EG and CLC-ER showed negligible excitation efficiency above 400 nm. Based on the quantum yields of CLC-P (17.53%), CLC-EG (12.4%), and CLC-ER (3.6%), the doping ratios were optimized, as shown in Fig. S10. The doping ratios of PTZ:EG 0.2 : 1.0 wt% (*R*-CLC-PG5) and 0.14 : 1.0 wt% (*R*/*S*-CLC-PG) were selected for CPL measurements. In *R*-CLC-PG5, a weak CPL signal was observed at 620 nm, whereas in *R*/*S*-CLC-PG (Table S1), the g_{lum} value at 620 nm was nearly zero. As a result, *R*/*S*-CLC-PG was chosen to demonstrate the ExD CPL behavior with different emission wavelengths. The CD spectra of CLCs-PG showed a clear stacking effect, combining the features of CLCs-P and CLCs-EG. The CD signals between 280 nm and 350 nm are attributed to the helical superstructure of the CLC host, and the peak handedness matched that of *R*/*S*-CLCs-P (Fig. 2). The CD peaks at 385 nm weakened due to the opposing dichroism of PTZ and EG. At longer wavelengths, the PTZ dye dominated, and the handedness aligned with that of *R*/*S*-CLCs-P.[56,57] The ExD CPL behavior is clearly shown in Fig. 3b, where the g_{lum} values shifted from −0.48/0.37 at 365 nm excitation to 0.53/−0.53 at 420 nm excitation (Fig. S11). This is due to the selective excitation of the achiral dyes. Under 365 nm light, both PTZ and EG were excited and the CPL of EG dominated. Under 420 nm irradiation, only PTZ was excited and inverted red CPL could be observed. The FL spectra and photographs at different excitation wavelengths, shown in Fig. S12–S14, further confirm the ExD CPL phenomenon in the CLCs.

The ratios of PTZ to ER (0.2 : 1.0 wt% for *R*-CLC-PR5, 0.14 : 1.0 wt% for *R*/*S*-CLC-PR, and 0.11 : 1.0 wt% for *R*-CLC-PR9) were selected for CPL measurements. The g_{lum} values shifted from −0.1 for *R*-CLC-PR5 to −0.16 for *R*-CLC-PR and −0.21 for *R*-CLC-PR9 as the PTZ ratio increased (Fig. S10 and 3d). This trend demonstrates the selective excitation mechanism underlying the ExD CPL behavior.[40] Based on the CPL intensity and emission characteristics at different excitation wavelengths, *R*/*S*-CLC-PR (Table S1) was chosen to exhibit the ExD CPL at a fixed wavelength. The CD spectra of CLCs-PR also showed a clear stacking effect from the CD spectra of CLCs-P and CLCs-ER (Fig. 3c). In the CPL spectra, the ExD phenomenon is clearly observed as shown in Fig. 3d. The g_{lum} values shift from −0.16/0.13 at 365 nm excitation to 0.52/−0.55 at 420 nm excitation (Fig. S11). Importantly, this switching behaviour occurs without significant attenuation, enabling potential long-term use (Fig. S15).

The POM images of the dual-dye-doped CLCs were examined to further investigate their superstructure in detail. Characteristic fingerprint textures were observed in these CLCs (Fig. 4), indicating that the highly ordered helical superstructures remained intact even after doping with more than one dye. The direction of the helix was then confirmed. As shown in Fig. 4c–f, the *R*-CLCs exhibited a right-handed structure, while the *S*-CLCs displayed a left-handed helix. These results demonstrate that the superstructure of the CLCs is unaffected by the achiral dyes. This finding further confirms that the ExD CPL of the CLCs can be engineered by doping achiral dyes with different dichroisms and excitation spectra.

By utilizing the ExD CPL properties of CLCs-PR, an information anti-counterfeiting device is proposed,[5,6] as shown in Fig. 5. The three LC inks (A, B, and C, representing *S*-CLC-P, *R*-CLC-P, and *S*-CLC-PR, respectively) all exhibited orange emission under UV light. Initially, different information was encoded using binary codes of standard 8-bit ASCII characters. Subsequently, the three CLC inks were injected into an 8 × 3 pixel array according to a predefined pattern. Under 365 nm

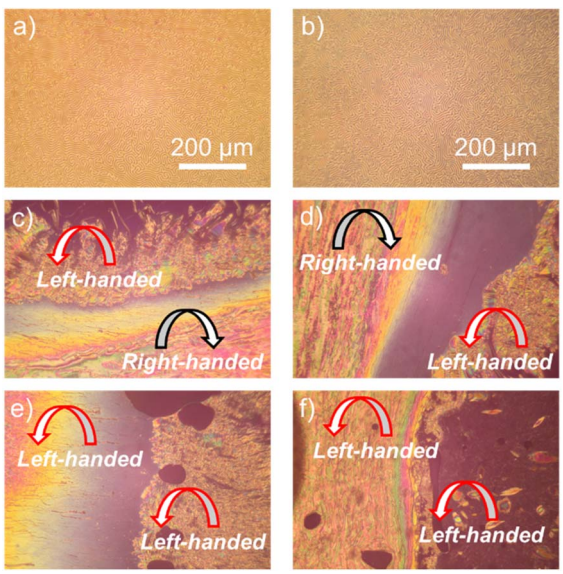

Fig. 4 POM images of (a) *R*-CLC-PG and (b) *R*-CLC-PR. The miscibility test of (c) *R*-CLC-PG, (d) *R*-CLC-PG, (e) *S*-CLC-PR and (f) *S*-CLC-PR with a cholesteryl oleyl carbonate.

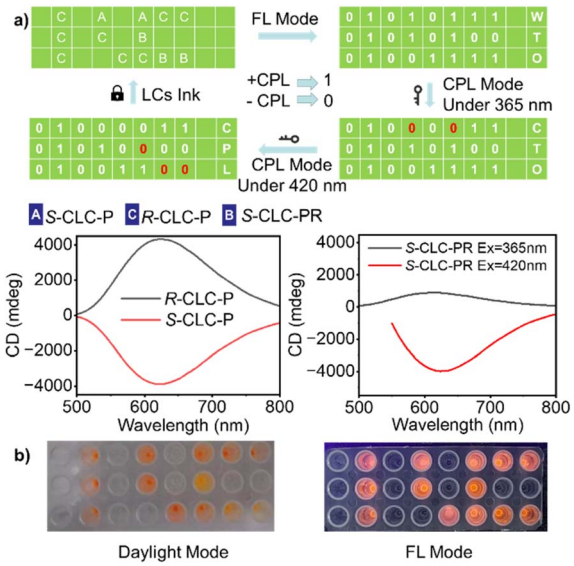

Fig. 5 (a) The schematic diagram of information coding using the *R*/*S*-P and *S*-CLC-PR system. (b) Daylight image and the FL mode image under excitation at 365 nm.

light, the message "WTO" could be easily detected in the fluorescence mode. We defined cells emitting L-CPL as outputting the number "1," while the others output "0." When the array was scanned using CP light analysis tools, the message "CTO" appeared under 365 nm UV light, and the actual information "CPL" could be obtained under 420 nm UV light. Fig. S16 presents the FL images obtained under 365 nm and 420 nm excitation wavelengths. Distinct intensity variations between samples are discernible under 365 nm illumination, whereas the 420 nm excitation exhibited diminished contrast due to pronounced background interference. Notably, the encrypted pattern could only be reliably deciphered through CPL detection, demonstrating enhanced security through wavelength-selective decryption.

A complementary anti-counterfeiting demonstration is illustrated in Fig. S17. The hierarchical pattern features *R*-CLC-PG-printed floral elements and *S*-CLC-EG-printed foliar components. Under 365 nm irradiation, the flower and leaf motifs exhibit yellow and green emission, respectively. Spectral modulation occurs under 420 nm excitation, with the floral component demonstrating a red emission while the foliar elements are non-emissive. Furthermore, the implementation of L-CPF enables dynamic FL intensity change, enabling a multi-level anti-counterfeiting system with spectral and polarization dual-responsive characteristics.

The security of the anti-counterfeiting labels is greatly enhanced by their higher complexity compared to traditional fluorescence codes. Furthermore, inspection is not overly difficult, requiring only different excitation light sources. In addition, these labels exhibit improved longevity, preventing failure during extended use. Together, these features highlight the potential of these labels as effective daily anti-counterfeiting solutions.

Conclusion

In conclusion, we have presented a strategy to achieve ExD CPL in a single CLC through selective excitation of achiral dichroic dyes with different dichroism and excitation wavelengths. When the excitation wavelength was changed from 365 nm to 420 nm, the CPL emission color of CLCs-PG shifted from green (530 nm) to red (620 nm), with an inversion of CP handedness. In CLCs-PR, the CP polarization inverted significantly without obvious change in the emission wavelength through emission wavelength design. Based on the experimental results and theoretical calculations, the selective excitation of different dichroic dyes is responsible for the ExD CPL. This study not only provides a versatile and widely applicable platform for constructing ExD CPL materials but also offers guidelines for developing materials for long-term, multilevel information anti-counterfeiting applications.

Author contributions

Lulu Li performed the experiment and data analysis and wrote the manuscript draft. Peiting Jiang and Lei Chen revised the manuscript. Yang Li and Yixiang Cheng conceived the ideas and designed the research, revised the manuscript and provided funding acquisition.

Conflicts of interest

There are no conflicts to declare.

Data availability

The data supporting this article have been included as part of the supplementary information (SI). The data that support the findings of this study are available from the corresponding authors, Yixiang Cheng and Yang Li, upon reasonable request. Supplementary information is available. See DOI: **https://doi.org/10.1039/d5sc07444d**.

Acknowledgements

This work was supported by the National Natural Science Foundation of China (22403019, 22302047, 92156014, and 52373188) and China Postdoctoral Science Foundation (2024M753177).

Notes and references

1 M. Zhang, C. Ma, J. Ma, Y. Yuan, J. Huang and Y. Yan, *J. Food Compos. Anal.*, 2025, **148**, 108240.
2 H. Ryu, B. H. Son, J. Kim, J. Kim and Y. H. Ahn, *Sensors*, 2025, **25**, 5160.
3 M. Unal and E. B. Cakici, *Microsc. Res. Tech.*, 2025, DOI: **10.1002/jemt.70061**.
4 W.-M. Yin, B. Dang, S. Guo, M. Sun, Y.-R. Guo, S. Liu, S. Li, J. Li, T. D. James and Z. Chen, *Nat. Commun.*, 2025, **16**, 7978.

5 S. Lin, Y. Tang, W. Kang, H. K. Bisoyi, J. Guo and Q. Li, *Nat. Commun.*, 2023, **14**, 3005.
6 S. Li, Y. Tang, Q. Fan, Z. Li, X. Zhang, J. Wang, J. Guo and Q. Li, *Light:Sci. Appl.*, 2024, **13**, 140.
7 Q. Feng, J. Yao, Q. Wu, Y. Qiu, Z. Wang, X. Wang, W. Chen, S. Tong, X. Cao, J. Sun, Q. Ye, J. Liu, D. Wang, J. Wang and H. Huang, *Chem. Sci.*, 2025, **16**, 17470.
8 Q. Guo, M. Zhang, Z. Tong, S. Zhao, Y. Zhou, Y. Wang, S. Jin, J. Zhang, H. B. Yao, M. Zhu and T. Zhuang, *J. Am. Chem. Soc.*, 2023, **145**, 4246.
9 L. Li, P. Jiang, X. Zhang and Y. Li, *Angew. Chem., Int. Ed.*, 2024, e202417149.
10 X. Yang, M. Zhou, Y. Wang and P. Duan, *Adv. Mater.*, 2020, **32**, e2000820.
11 J. Huang, X. Yang, X. Jin, H. Yang and P. Duan, *Nano Res.*, 2025, **18**, 94907182.
12 Y. Li, S. Deng, Y. Li, H. Tang, Z. Chen, J. Xie, F. Song and W. Huang, *Small*, 2025, **21**, 2502819.
13 L. E. MacKenzie, L.-O. Pålsson, D. Parker, A. Beeby and R. Pal, *Nat. Commun.*, 2020, **11**, 1676.
14 Y. Bai, Z. Yang, Q. Deng, H. Zan, S. Cao, X. Han, M. Yuan, T. Chang and R. Zeng, *Angew. Chem., Int. Ed.*, 2025, **64**, e202509283.
15 W.-M. He, J. Zha, Z. Zhou, Y.-J. Cui, P. Luo, L. Ma, C. Tan and S.-Q. Zang, *Angew. Chem., Int. Ed.*, 2024, **63**, e202407887.
16 D.-Y. Liu, H.-Y. Li, R.-P. Han, H.-L. Liu and S.-Q. Zang, *Angew. Chem., Int. Ed.*, 2023, **62**, e202307875.
17 S. Basu, M. Perić Bakulić, Ž. Sanader Maršić, V. Bonačić-Koutecký and N. Amdursky, *ACS Nano*, 2023, **17**, 16644–16655.
18 H. Liu, D.-D. Ren, P.-F. Gao, K. Zhang, Y.-P. Wu, H.-R. Fu and L.-F. Ma, *Chem. Sci.*, 2022, **13**, 13922–13929.
19 H. Li, J. Gu, Z. Wang, J. Wang, F. He, P. Li, Y. Tao, H. Li, G. Xie, W. Huang, C. Zheng and R. Chen, *Nat. Commun.*, 2022, **13**, 429.
20 X.-X. Guo, J.-H. Chen, J.-B. Luo, J.-H. Wei, Z.-Z. Zhang, Z.-L. He, Q.-P. Peng and D.-B. Kuang, *Adv. Opt. Mater.*, 2024, **12**, 2400681.
21 D. Chen, F. Xie, X. Lv, Y. Zhang and Y. Liang, *J. Mater. Chem. C*, 2025, **13**, 5788.
22 J. Wang, T. Yin and J. Ge, *Small*, 2024, **20**, 2311308.
23 X. Chen, Y. Wu, B. Tian, K. Zheng, H. Zhan and W. Wu, *Adv. Funct. Mater.*, 2024, **34**, 2316487.
24 C. Xue, Y. Jiang, H.-X. Wang, C. Du, L. Xu, T. Li and M. Liu, *Angew. Chem., Int. Ed.*, 2022, **61**, e202205633.
25 W. Hao, Y. Wang and M. Liu, *ACS Mater. Lett.*, 2024, **6**, 3487–3495.
26 H.-R. Fu, R.-Y. Zhang, T. Li, C.-Y. Wei, S. Liu, J.-Y. Xu, X. Zhu, J. Wei, Q.-R. Ding and L.-F. Ma, *Chem. Commun.*, 2024, **60**, 10212–10215.
27 Z. Man, Z. Lv, Z. Xu, M. Liu, J. He, Q. Liao, J. Yao, Q. Peng and H. Fu, *J. Am. Chem. Soc.*, 2022, **144**, 12652–12660.
28 J. J. M. Hurley and L. Zhu, *J. Phys. Chem. A*, 2022, **126**, 5711–5720.
29 Y. Zhang, H. Yang, H. Ma, G. Bian, Q. Zang, J. Sun, C. Zhang, Z. An and W. Y. Wong, *Angew. Chem., Int. Ed.*, 2019, **58**, 8773–8778.
30 K. Yao, Z. Liu, H. Li, D. Xu, W.-H. Zheng, Y.-W. Quan and Y.-X. Cheng, *Sci. China:Chem.*, 2022, **65**, 1945–1952.
31 Y. Wu, C. Yan, X.-S. Li, L. H. You, Z.-Q. Yu, X. Wu, Z. Zheng, G. Liu, Z. Guo, H. Tian and W.-H. Zhu, *Angew. Chem., Int. Ed.*, 2021, **60**, 24549–24557.
32 O. Oki, C. Kulkarni, H. Yamagishi, S. C. J. Meskers, Z.-H. Lin, J.-S. Huang, E. W. Meijer and Y. Yamamoto, *J. Am. Chem. Soc.*, 2021, **143**, 8772–8779.
33 J. Luo, Y. Li, H. Li, Q. Li and Y. Cheng, *ACS Mater. Lett.*, 2024, **6**, 2957–2963.
34 Y. Li, Y. Chen, J. Luo, Q. Li, Y. Quan and Y. Cheng, *Chin. Chem. Lett.*, 2024, 109864.
35 L. Gu, H. Wu, H. Ma, W. Ye, W. Jia, H. Wang, H. Chen, N. Zhang, D. Wang, C. Qian, Z. An, W. Huang and Y. Zhao, *Nat. Commun.*, 2020, **11**, 944.
36 A. Li, D. Zheng, M. Zhang, B. Wu and L. Zhu, *Langmuir*, 2020, **36**, 8965–8970.
37 Y. Liu, S. Yang, B. Zhao and J. Deng, *ACS Macro Lett.*, 2023, **12**, 530–535.
38 Y. Zhang, Y. Li, Y. Quan, S. Ye and Y. Cheng, *Angew. Chem., Int. Ed.*, 2023, **62**, e202214424.
39 Y. Li, Y. Chen, H. Li, C. Liu, L. Li, Y. Quan and Y. Cheng, *Angew. Chem., Int. Ed.*, 2023, **62**, e202312159.
40 Y. Chen, Y. Zhang, H. Li, Y. Li, W. Zheng, Y. Quan and Y. Cheng, *Adv. Mater.*, 2022, **34**, 2202309.
41 X. Li, W. Hu, Y. Wang, Y. Quan and Y. Cheng, *Chem. Commun.*, 2019, **55**, 5179–5182.
42 Y. Chen, Z. Xu, W. Hu, X. Li, Y. Cheng and Y. Quan, *Macromol. Rapid Commun.*, 2021, **42**, 2000548.
43 W. J. Newsome, S. Ayad, J. Cordova, E. W. Reinheimer, A. D. Campiglia, J. K. Harper, K. Hanson and F. J. Uribe-Romo, *J. Am. Chem. Soc.*, 2019, **141**, 11298–11303.
44 Y. Tsutsui, W. Y. Zhang, S. Ghosh, T. Sakurai, H. Yoshida, M. Ozaki, T. Akutagawa and S. Seki, *Adv. Opt. Mater.*, 2020, **8**, 1902158.
45 J. Y. Gong, J. L. Han, Q. Liu, X. J. Ren, P. F. Wei, L. Yang, Y. Zhang, J. Liu, Y. Q. Dong, Y. G. Wang, X. Z. Song and B. Z. Tang, *J. Mater. Chem. C*, 2019, **7**, 4185–4190.
46 J. E. Kwon, S. Park and S. Y. Park, *J. Am. Chem. Soc.*, 2013, **135**, 11239–11246.
47 M. G. Debije, C. Menelaou, L. M. Herz and A. P. H. J. Schenning, *Adv. Opt. Mater.*, 2014, **2**, 687–693.
48 M. T. Sims, L. C. Abbott, R. J. Mandle, J. W. Goodby and J. N. Moore, *Phys. Chem. Chem. Phys.*, 2023, **25**, 10367–10383.
49 K. Yao, Y. Shen, Y. Li, X. Li, Y. Quan and Y. Cheng, *J. Phys. Chem. Lett.*, 2021, **12**, 598–603.
50 G. Albano, G. Pescitelli and L. Di Bari, *Chem. Rev.*, 2020, **120**, 10145–10243.
51 C. Wang, Q. Qiao, W. Chi, J. Chen, W. Liu, D. Tan, S. McKechnie, D. Lyu, X. F. Jiang, W. Zhou, N. Xu, Q. Zhang, Z. Xu and X. Liu, *Angew. Chem., Int. Ed.*, 2020, **59**, 10160–10172.
52 Y. Shi, J. Han, C. Li, T. Zhao, X. Jin and P. Duan, *Nat. Commun.*, 2023, **14**, 6123.
53 Q. H. Li, G. Zou, D. Li, C. Liu, W. T. Gao, Y. Li and Y. X. Cheng, *Adv. Opt. Mater.*, 2024, **12**, 2303185.

54 K. Akagi, T. Yamashita, K. Horie, M. Goh and M. Yamamoto, *Adv. Mater.*, 2020, **32**, e1906665.
55 K. Akagi, *Chem. Rev.*, 2009, **109**, 5354–5401.
56 Y. Zhang, W. Yu, H. Li, W. Zheng and Y. Cheng, *Chem.–Eur. J.*, 2023, **29**, e202204039.
57 J. Liu, Z.-P. Song, L.-Y. Sun, B.-X. Li, Y.-Q. Lu and Q. Li, *Responsive Mater.*, 2023, **1**, e20230005.